ChemBioChem

Research Article
doi.org/10.1002/cbic.202400759

Chemistry
Europe
European Chemical
Societies Publishing

www.chembiochem.org

Ferrocenyl β-Diketonate Compounds: Extended Ring Systems for Improved Anticancer Activity

Benjamin J. Hofmann,[a, b] Enas T. Aljohani,[a] Natalia Cicovacki,[a] Ivan Lee,[a] Derek T. Warren,[a] Anastasia Sobolewski,[a] Tameryn Stringer,[a, c] and Rianne M. Lord*[a, b]

A library of ferrocenyl β-diketonate compounds with varying degrees of aromatic functionality have been synthesized and fully characterized. This includes cyclic voltammetry and the analysis of four new structures by single crystal X-ray diffraction. The compounds cytotoxic potential has been determined by MTT screening against pancreatic carcinoma (MIA PaCa-2), ovarian adenocarcinoma (A2780), breast adenocarcinomas (MDA-MB-231 and MCF-7) and normal epithelial retinal (ARPE-19). The compounds show a general trend, where increasing the number of aromatic rings in the molecule yields an increase in cytotoxicity and follows the trend anthracenyl > naphthyl >

phenyl > methyl. The compounds are particularly sensitive to the triple negative cancer cell line MDA-MB-231, and the potential modes of action have been studied by production of reactive oxygen species using fluorescence microscopy and cell morphology using Scanning Electron Microscopy. All assays highlight the ferrocenyl β-diketonate with an anthracenyl substituent to be the lead compound in this library. The decomposition of this compound was also observed within cells, yielding a cytotoxic fluorescent molecule, which has been visualized by confocal microscopy.

Introduction

Iron is a bio-essential metal for human growth and development. It is mainly found in hemoglobin for oxygen transport, but also in storage compounds, e.g., ferritin and hemosiderin, myoglobin, a protein that provides oxygen to muscles, in DNA synthesis, detoxifying enzymes, and electron transport processes.[1] Even though it is the fourth most abundant element, absorption of iron is poor and leads to lower bioavailability, and chelating agents are often employed to increase the elements availability.[2] Due to its importance in the body, lower toxicity levels, known metabolic and excretion pathways, abilities to switch between Fe(II) and Fe(III), and unique modes of action due to Fenton-type mechanisms (can cause cell death by reactive oxygen species (ROS)),[3] iron has been frequently studied for its use in chemotherapy.

Ferrocene is an iron-based organometallic compound and is one of the most stable and utilized organometallic moieties. It has low toxicity and favorable reversible oxidation-reduction

behavior, making it useful for controlling electron transfer processes. Ferrocene and its derivatives have many applications, for example as fuel additives and materials chemistry, however, they have been heavily researched in the last three decades for their medicinal applications.[4] There have been a plethora of ferrocene containing compounds which have shown impressive anti-infective activity[5] and anticancer activity,[6] where changes in oxidation state or functionalization of the cyclopentadienyl (Cp) rings have led to improved solubility.[7] For example, ferrocenium salts with picrate (Figure 1, A.1) and trichloroacetate (Figure 1, A.2) have improved solubility and exhibit high anticancer activity,[8] which was likely attributed to the generation of ROS and DNA interactions. The most notable ferrocene containing anticancer compounds are the ferrocifens

[a] B. J. Hofmann, E. T. Aljohani, N. Cicovacki, I. Lee, D. T. Warren, A. Sobolewski, T. Stringer, R. M. Lord
School of Chemistry, Pharmacy and Pharmacology, University of East Anglia, Norwich, Norfolk NR4 7TJ, UK

[b] B. J. Hofmann, R. M. Lord
Department of Chemistry, University of Warwick, Coventry CV4 7SH, UK
E-mail: rianne.lord@warwick.ac.uk

[c] T. Stringer
School of Chemistry, University of Waikato, Hamilton 3240, New Zealand
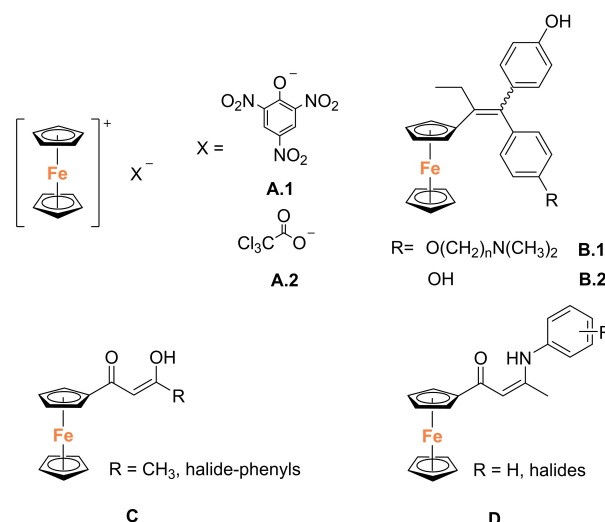
Figure 1. Bioactive ferrocene-based anticancer compounds A–D.

ChemBioChem

Research Article
doi.org/10.1002/cbic.202400759

Chemistry Europe
European Chemical
Societies Publishing

(e.g., Figure 1, B.1–2), which are based on the well-known breast cancer drug tamoxifen.[9] Such ferrocifens are selective estrogen receptor modulators (SERMs) and can help to target aggressive forms of breast cancer.[10] Since these studies, there has been many other ferrocene compounds containing amides, amines, amino acids, phenols, heterocycles and known active drugs, which have been readily reviewed for their bioactivity.[6]

Compounds based on β-diketonates are of interest, as the fragment can be found in many biologically active metallodrugs such as Budotitane[11] and vanadyl acetylacetone,[12] or in bioactive natural products, e.g., curcumin.[13] In 2020, we reported ferrocenyl β-diketonate compounds (Figure 1C) which had superior anticancer activity compared to the ferrocenyl β-ketoimine compounds (Figure 1D),[14] and noted the inclusion of the ferrocenyl moiety improved the activities of the compounds by >16-fold. The compounds were sensitive towards the triple negative breast cancer cell line MDA-MB-231, when compared to hormone-dependent cell line MCF-7. We have also synthesized bimetallic ferrocene-ruthenium compounds with ferrocenyl β-diketonate ligands, e.g., piano-stool compounds[15] and coordination compounds,[16] and have shown that the ferrocene significantly improves the activity and uptake of the molecules. Importantly, for all libraries we observed general trends in the number of aromatic substituents on the ferrocenyl β-diketonate compounds, where the increase in number of rings led to an increase in cytotoxicity and followed the trend naphthyl > phenyl > methyl. The compound library was limited and the modes of action of the ferrocenyl β-diketonate compounds were not widely studied, therefore, we report herein nine (six new) ferrocenyl β-diketonate compounds with increasing aromaticity and assess how the number of aromatic rings effects their bioactivity in cancer cells.

Results and Discussion

Synthesis and Characterization

The synthesis of ferrocenyl β-diketonate compounds **1**, **2** and **4** have been previously reported.[14–16] Following a slightly modified procedure (under inert atmosphere), compounds **3**, **5**–**8** have been synthesized herein (Scheme 1). The anthracenyl compound **9** was not accessible via the standard protocol and was synthesized by deprotonating acetyl ferrocene with sodium bis(trimethylsilyl)amide and reacting it with anthracene-9-carboxylic acid chloride at 0 °C (Scheme 1).[17] All compounds were obtained in low to moderate yields and have been fully characterized by NMR and IR spectroscopy, elemental analysis, cyclic voltammetry, high resolution mass spectrometry (HRMS), and single crystal X-ray diffraction (scXRD) where possible.

These compounds can exist as the enol and diketone forms, and we observed these as major and minor products, respectively, in the ¹H NMR spectra. For compounds **3**, **5** and **7** which contain a sp^3-carbon at the substituent, a rather high fraction of keto is observed, between 19–22%. In contrast, for the aryl and naphthyl substituted compounds **6** and **8**, only 6–7% of the keto form is observed, whilst no keto form is
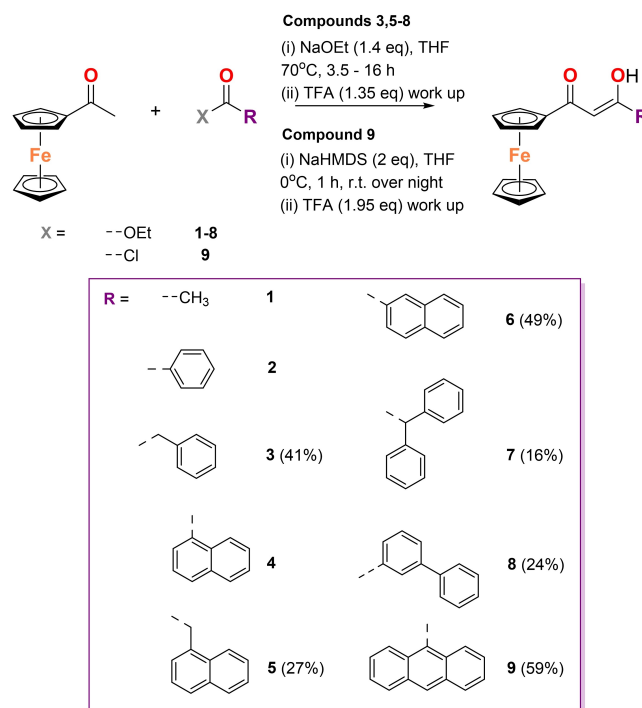
Scheme 1. Synthetic method for ferrocenyl β-diketonate compounds 3, 5–9.

observed for the anthracenyl substituted compound **9**. In all cases, the successful formation can be determined by the appearance of the methine singlet proton between 7.0–5.7 ppm (enol), and the splitting of the protons in the region of 5.3–4.2 ppm due to the Cp rings, where the unsubstituted Cp ring appears as a five-proton singlet and the substituted Cp appears as two sets of two-proton triplets. ¹³C{¹H} NMR is also a useful tool for determining successful formation, with the keto/enol quaternary carbons being observed between 205–180 ppm and the methine *C*H (enol) between 105.0–94.0 ppm (Figures S1–S12).

The IR spectra of all compounds reveal a broad band between 1660–1500 cm⁻¹ with multiple peaks due to the combination of C=O stretch vibrations in the hydrogen bonded six-membered ring of the β-diketonate functionality, which is overlayed with the C–H(acac) in-plane bend mode. While the $\tilde{v}$ (C=O) vibrations are less characteristic, the successful synthesis of the compounds is observed by the presence of the characteristic ferrocenyl Cp–Fe–Cp stretch and bend modes between 500–463 cm⁻¹ (Figures S13–S22). HRMS analysis was conducted on all new samples and show peaks corresponding to both $[M]^+$ and $[M+Na]^+$. All spectra are shown in Figures S23–S28 of the *Supporting Information*.

The electrochemistry of compounds **3**–**9** has been investigated in a 0.1 M solution of tetrabutylammonium hexafluorophosphate in acetonitrile and all values given are referenced to the standard calomel electrode (SCE) using a ferrocene standard (compounds **1** and **2** have been previously reported[15]). All compounds exhibit a reversible redox couple with $E_{1/2}$ between 0.63–0.66 V assigned to the ferrocene/ferrocenium couple in line with previously reported functional-

ChemBioChem

Research Article
doi.org/10.1002/cbic.202400759

Chemistry
Europe
European Chemical
Societies Publishing

ized ferrocenyl β-diketonates (Table 1 and Figures S34–S40, *Supporting Information*). An example voltamogram is shown in Figure 2 for compound **3**. Even though, the highest oxidation potential is observed for the anthracenyl functionalized compound **9**, no general trends can be deduced between alkyl and aryl functionalized compounds, demonstrating their negligible electronic effect on the ferrocenyl moiety. Aside of the reversible Fc′/Fc′+ redox couple, the cyclic voltammograms of all compounds show a reduction at potentials below −1.53 V assigned to the organic part of the β-diketonates. The potential and reversibility are highly dependent on the functionality, with alkyl substituents (**3**, **5**, **7**) being irreversibly reduced at significantly lower reduction potentials ($E_{PC} = -1.90--1.94$ V), whilst aryl or naphthyl substituted compounds (**4**, **6**, **8**) are *quasi*-reversibly reduced at higher potentials with E_{PC} between −1.65−−1.70 V. In contrast, the anthracenyl functionalized compound **9** is irreversibly reduced at the highest potential with $E_{PC} = -1.53$ V in line with its ability to stabilize radicals as known from Birch-type reductions.[18]

Red/orange single crystals suitable for single crystal X-ray diffraction (scXRD) analysis were obtained for compounds **3**, **5**, **6** and **7** (CSD: 2375601–2375604).[19] The crystals were grown by slow evaporation of a concentrated acetone solution at room temperature, and structural solutions performed in monoclinic (**3**, **5**, **7**; $P2_1/c$) or orthorhombic (**6**; $Pna2_1$) space groups. The molecular structures are shown in Figure 3. Compound **1** has already been reported,[14] however, another space group ($P2_1/c$) was obtained and the data is provided in Figure S29 and Table S2 (CSD: 2383116) of the *Supporting Information*.[19] All molecules display a planar structure around the enol/keto center with angles ranging from 119.56(14)–122.05(19)° (Table 2) and in all cases, an intramolecular hydrogen bond is observed between enol–keto with O–H…O distances ranging between 1.699 and 1.794 Å (D–H…A), thus restraining the geometry to a planar orientation. The ferrocenyl Cp ligands also adopt geometries close to an eclipsed arrangement, which was observed in our previous work. Several of the compounds have interesting intermolecular interactions, including interactions between the $\pi_{phenyl}…HC_{Fc}$, $CH_{Fc} …HC_{Fc}$, $\pi_{phenyl}…OH$, and CO… HC_{phenyl}, with packing images shown in Figures S30–S33 (all scXRD data is stated in Table S1).

Figure 3. Molecular structures of compounds **3**, **5**, **6** and **7**, with ellipsoids placed at the 50% probability level.

Table 1. Electrochemical data for compounds **1**–**9**. Potentials are corrected using ferrocene as internal standard with $E_{1/2} = 0.40$ V against SCE. Peaks associated with the irreversible (only E_{PC}) or *quasi*-reversible reduction (E_{PC} and E_{PA}) of the organic part of the β-diketonate moiety are given (E^{red}).[15]

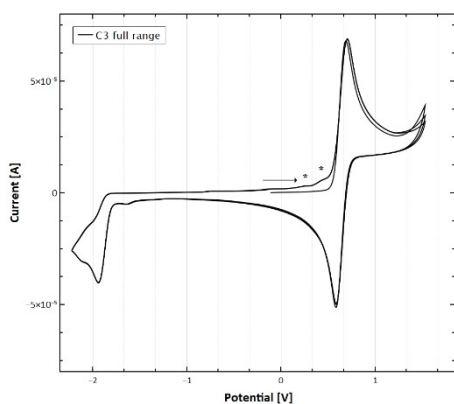| Compounds	$E_{1/2}$ (Fc′/Fc′+) [V]	E_{PC}^{Red} [V]	E_{PA}^{Red} [V]
1	0.63[15]	n.d.	n.d.
2	0.63[15]	n.d.	n.d.
3	0.64	−1.94	–
4	0.64	−1.68	−1.60
5	0.65	−1.94	–
6	0.63	−1.65	−1.57
7	0.64	−1.90	–
8	0.64	−1.70	−1.62
9	0.66	−1.53	–

Figure 2. An example cyclic voltammogram of compound **3** in a solution of 0.1 M TBAPF₆ in acetonitrile, using a scanning speed of 0.1 V/s and referenced to ferrocene $E^{0′}$ (Fc/Fc⁺ = 0.40 V against SCE) as internal standard. *Signals derived from electrochemically produced decomposition products.
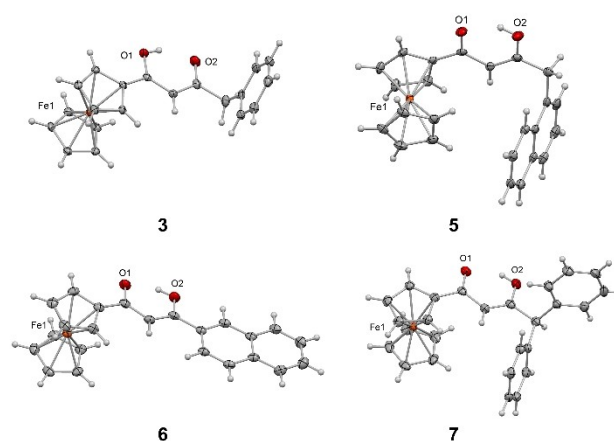
Table 2. Selected bond lengths and angles for compounds **3**, **5**, **6** and **7**, s.u.s are shown in parenthesis.

Compounds	**3**	**5**	**6**	**7**
Bond Lengths (Å)				
O1–C1	1.3195(16)	1.282(3)	1.2771(19)	1.255(2)
C1–C2	1.3859(18)	1.426(3)	1.418(2)	1.447(3)
C2–C3	1.4154(19)	1.372(4)	1.385(2)	1.357(3)
C3–O2	1.2685(17)	1.319(3)	1.3104(18)	1.332(2)
Fe1–Cg1	1.648	1.639	1.647	1.635
Fe1–Cg2	1.649	1.653	1.654	1.650
Bond Angles (°)				
O1–C1–C2	121.40(12)	120.5(2)	121.84(14)	121.14(17)
C1–C2–C3	120.40(12)	120.0(2)	119.56(14)	121.06(18)
C2–C3–O2	122.09(13)	121.1(2)	120.05(15)	122.05(19)

ChemBioChem

Research Article
doi.org/10.1002/cbic.202400759

Chemistry Europe
European Chemical
Societies Publishing

Cell Viability Assays

Chemosensitivity studies were performed using an MTT assay after human cell lines: pancreatic carcinoma (MIA PaCa-2), ovarian adenocarcinoma (A2780), breast adenocarcinomas (MDA-MB-231 and MCF-7) and normal epithelial retinal (ARPE-19) were incubated with cisplatin (CDDP) and ferrocenyl β-diketonate compounds **1–9** for 96 hours. The IC_{50} values ± SD for all compounds after triplicate repeats (n = 9) are shown in Figure 4. A general trend is observed for all cell lines where the addition of aromatic rings to the molecules improves their cytotoxicity. Compound **1** with no aromatic substituents has the lowest cytotoxicity, whilst compound **9**, which has three aromatic rings, is the most potent compound in the series. All IC_{50} values are state in Table S3 of the *Supporting Information*.

Compounds were also screened against the normal retinal epithelial cell line, ARPE-19, to determine the possibility of cancer cell selectivity. The compounds all have moderate cytotoxicity against this cell line (Table S4 and Figure S53). The most notable selectivity is observed for compounds **4** (R = 1-naphthyl) and **9** (R = 9-anthracenyl), where the selectivity index ranges from 1.50–4.02 and 1.34–3.49, respectively. Since ferrocene-based compounds have shown importance in the treatment of breast cancer, we were interested to see if these ferrocenyl β-diketonate compounds could target breast cancer, especially the difficult to treatment triple negative breast cancers (e.g., MDA-MB-231). The results against MCF-7 and MDA-MB-231 were similar in most cases. However, compound **9** has > 2.4-fold increased selectivity for MDA-MB-231 and IC_{50} values up to 4x higher than CDDP.

Stability Studies

Stability studies have been assessed by ^1H NMR spectroscopy over the 96 hours in both 100% $(CD_3)_2SO$ and in 90% $(CD_3)_2SO$ and 10% D_2O (Figures S41–S52). The ferrocenyl β-diketonate compounds **1–9** (**1**, **2** and **4** were previously reported) were analyzed after initial dissolution (ca. 5 min), 20 and 40 minutes

and then between 1 hour and 96 hours at 293 K (ca. 5 mg/mL). On analysis of the spectra, compounds **1–8** in both 100% $(CD_3)_2SO$ and 90% $(CD_3)_2SO$ and 10% D_2O, decompose between 2–6 hours to give free Cp (6.5 ppm) and a paramagnetic species, which is tentatively assigned to an Fe(III) species. This is comparable to our previously observations, however, these new compounds appear to decompose faster, where other compounds were stable for approximately 12 hours.[15] Compound **9** is the least stable and decomposes completely in the presence of water in < 2 hours.

Determination of Reactive Oxygen Species

Many chemotherapeutic drugs are known to induce cellular ROS and thus is a plausible mechanism of action for these ferrocenyl complexes, as they can easily and reversibly cycle between Fe(II) and Fe(III). To gauge whether the complexes can promote cellular ROS formation, the cell permeable fluorescein, 2′,7′-dichlorodihydrofluorescein diacetate (H_2DCFDA) was used as it deacetylates by esterase and oxidized by ROS to form fluorescent dichlorofluorescein (DCF).[20] Compounds **1**, **2**, **4** and **9** show good cytotoxicity trends against MDA-MB-231 cells, and were selected for additional studies. Firstly, MTT assays were conducted at 24 hours and show that all compounds exhibit moderate to low toxicity (IC_{50} ranging from 35.0 ± 0.4 μM to > 100 μM, Table S2). MDA-MB-231 cells were then dosed with 100 μM of each compound for 2 hours and ROS production measured using fluorescence microscopy. The results are shown in Figure 5. The untreated control sample (A) exhibits some fluorescence and this is suggestive of intrinsic ROS formation, which is considered to be a normal by-product of cancer cellular processes.[21] Like the control, CDDP (B) does not show any elevated ROS production at this concentration and time. However, MDA-MB-231 cells treated with compounds **1** (C), **2** (D) and **4** (E) show significant increases in ROS production. This contrasts with the results obtained for compound **9** (F), which shows only a small amount of ROS production, and this is in
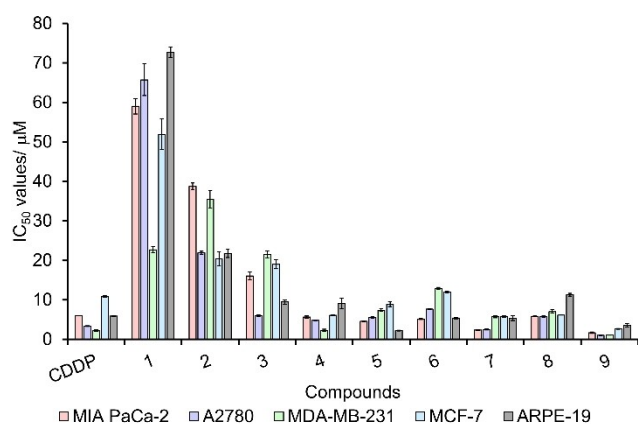

Figure 4. IC_{50} values ± SD of CDDP and compounds **1–9** when screened against MIA PaCa-2, A2780, MDA-MB-231, MCF-7 and ARPE-19 cell lines. All values are after 96 hours incubation (n = 9).

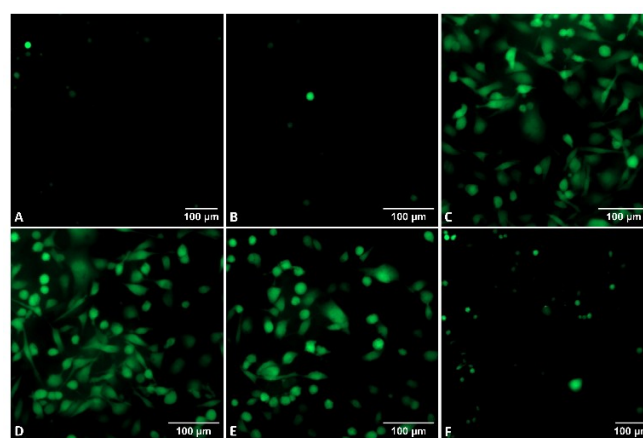**Figure 5.** Fluorescence images showing ROS production in MDA-MB-231 cells after treatment for 2 hours with (A) 0.4% DMSO (control) and 100 μM of (B) CDDP, (C) **1**, (D) **2**, (E) **4**, (F) **9**. Scale bar = 100 μm.

ChemBioChem

Research Article
doi.org/10.1002/cbic.202400759

Chemistry Europe
European Chemical
Societies Publishing

line with the lower stability (decomposition < 2 hours) observed in the NMR studies.

Cell Morphology by Scanning Electron Microscopy

MDA-MB-231 cells were incubated with compounds **1**, **2**, **4**, **9** and CDDP (including an untreated control) at 100 μM for 2 hours, before the samples were fixed and images captured using Scanning Electron Microscopy (SEM). Although ROS was observed after just 2 hours of incubation at 100 μM (Figure 5), no cell morphology changes were observed for compounds **2**, **4**, **9** and CDDP (Figure 6 and Figures S54–59). For example, the cells retain their characteristic features, such as expression of microvilli on the surface, microvesicles close to the surface and both filopodia (e.g., white arrows in Figure 6b) and lamellipodia (e.g., black arrow in Figure 6a) are still present.[22] Also, a similar distribution of the three typical phenotypes (globular, "cobble-stone" and squid shaped) were observed in all samples (Table S5).

These observations also follow the low cytotoxicity of the compounds at shorted incubation times (IC$_{50}$ > 100 μM at 24 hours, Table S3) and highlight the concentration and time are not sufficient to observe any cell apoptosis, despite the elevated ROS level detected at the same concentration and time. In contrast, compound **1** has moderate short-term cytotoxicity (IC$_{50}$ = 35.0 ± 0.4 μM at 24 hours, > 100 μM at 2 hours) and this was observed in the SEM images, where several cells show first signs of cellular stress. Cell shrinkage is evident and the lamellipodia have retracted, while the filopodia are left behind, which is usually indicative of the cell detaching from the culture vessel, and this could be induced by treatment with compound **1** (Figure 6c). Consequently, at least compound **1** is capable to produce sufficient high levels of ROS to induce morphological changes which might be assigned to its higher stability and therefore higher turnover number of the reversible
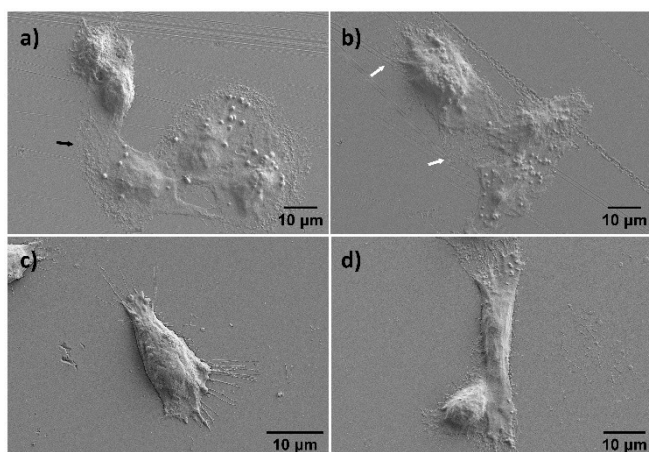
Fe(II)/Fe(III) redox couple which is thought to be the origin of the detected ROS.

Cell Free Fluorescence Measurements

As compound **9** contains an anthracenyl moiety, its fluorescence capabilities have been studied. However, when coupled to the ferrocenyl, the fluorescence was quenched in line with ferrocenes great ability to quench excited states.[23] On analysis of the stability studies, it was noticed the compound increased in fluorescence intensity over time. Coupled with the NMR findings (Figure S41–S52), we attribute this to the decomposition of the ferrocenyl moiety, which is prompted by the oxidation of the Fe(II) to Fe(III). The excitation spectrum of the decomposition product of compound **9** also exhibits the anthracene typical pattern with its strong absorption bands at 385, 365, 348 and 332 nm (Figure 7a), red-shifted by 5 nm when compared to anthracene (Figure S60). In contrast to anthracene, the emission band of the decomposition product of **9** is significantly broadened and exhibits a maximum at 460 nm and a shoulder at 485 nm. The maximum is less red-shifted than the non-ferrocenyl substituted compound 1-(9-anthryl)butane-1,3-dione (539 nm in ethanol),[24] however, it is at an adequate wavelength to use it as probe in confocal microscopy. To test
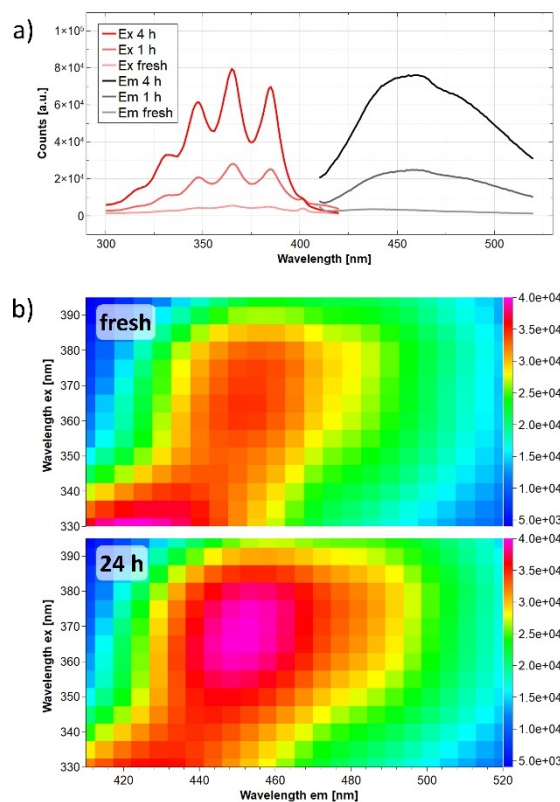
Figure 7. a) Spectra recorded after excitation (@455 nm) and emission (@365 nm) of compound **9** (20 μM) after preparation in neat DMSO (10 min), 1 and 4 hours; b) Fluorescence heat maps of compound **9** in freshly prepared complete RPMI medium (10 min) and after 24 hours.

Figure 6. Scanning Electron Microscopy (SEM) images of MDA-MB-231 cells after treatnebt for 2 hours with a) 0.4% DMSO (control), and 100 μM of b) CDDP, c) **1**, d) **9**. Examples for lamellipodia and filopodia are labelled with black and white arrows, respectively.

whether the increase in fluorescence is strong enough for live cell imaging, a sample of compound **9** in supplemented RPMI medium was prepared and fluorescence spectra were measured multiple times within 24 hours (Figure 7b and Figure S61). Excitation/emission maps are used to visualize the change of the fluorescence over time. The fluorescence heat map after 10 minutes is very similar to the map of DMSO spiked RPMI medium (Figure S62), however by addition of compound **9**, the autofluorescence is significantly diminished which might be attributed to both, the previously discussed ability of ferrocenyl compounds to quench luminescence and the inner filter effect. After 4 hours, increased emission is observed especially in the region between 360–380/450–465 nm (ex/em) and intensifies after 24 hours, however the increase in intensity is rather low with 3% and 15%, respectively, due to the strong autofluorescence of the medium.

Fluorescence Measurements in Cells by Confocal Microscopy

Due to the observed decomposition of compound **9** to a fluorescent molecule, MDA-MB-231 cells were incubated with **9** at 100 μM for 1, 2 and 4 hours, and analyzed by confocal microscopy (Figure 8 and Figure S63) to determine cellular uptake. For excitation, the laser with shortest wavelength available (400 nm) is used, however, due to the low extinction coefficient of **9** at this wavelength a relatively high laser power (2.00%) and post-processing is required to obtain a good contrast. The parameters used result in a minor autofluorescence visible in the control samples (Figure 8a, top). The compound **9** treated samples exhibit a significantly increased

fluorescence in the whole cell (Figure 8a, bottom), but additional studies would be required to determine its location and possible cellular targets. To test whether the fluorescence increases after longer incubation times (as observed during the fluorescence decomposition experiments), the fluorescence intensities per cell area of compound **9** (ex/em 400/452 nm) were measured for the control experiment and after 1, 2 and 4 hours (Figure 8b). For all samples a statistically significant increase of fluorescence was observed when compared to the control experiment. When comparing the samples at different incubation times, the fluorescence intensity does not change significantly, demonstrating that the uptake is fast, and the final cellular concentration of the fluorescent probe is obtained within 1 hour. No correlation between the rate of decomposition and fluorescence intensity is observed which is highly likely due to the use of PFA as fixing agent and the rather long processing time necessary to stain and prepare the samples. While similar uptake studies have shown that fluorescent acetylacetonate complexes are viable probes to determine the cellular distribution by incorporation in lanthanum[25] and vanadium complexes,[26] these results demonstrate that the highly toxic ferrocenyl functionalized compound **9**, and possibly its derivatives, are viable tools for the design of metallodrugs to increase their activity combined with fluorescent properties.

Conclusions

We report herein nine (six new) ferrocenyl β-diketonate compounds, **1**–**9**, which have varying numbers of aromatic substituents. The compounds have been fully characterized by
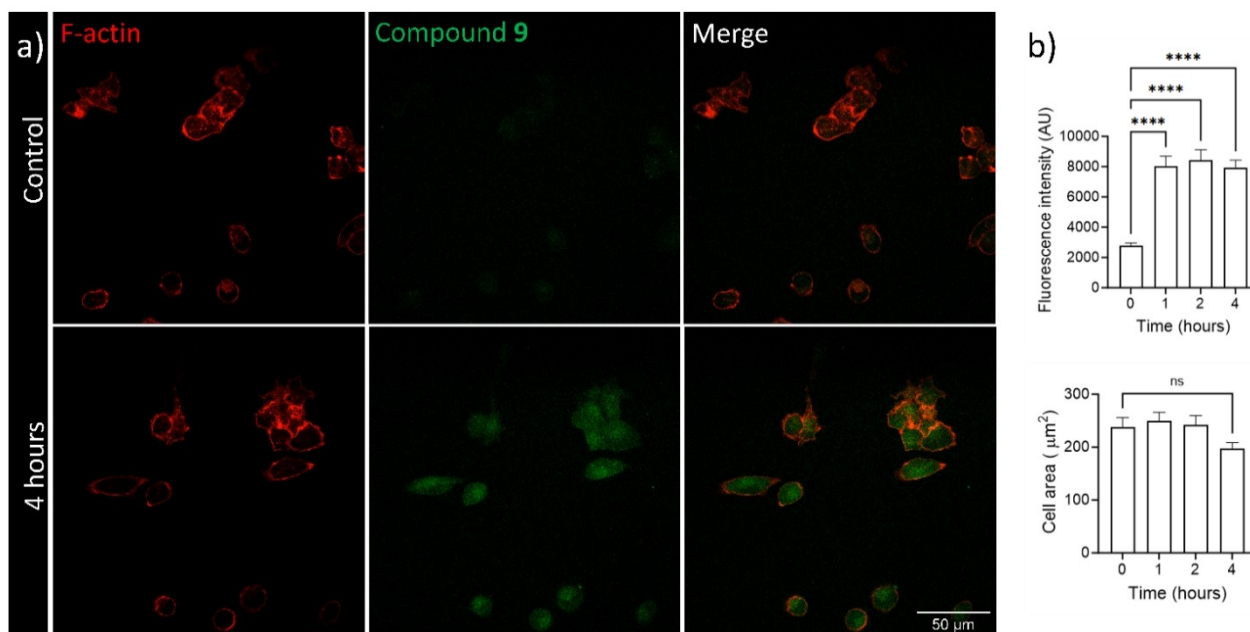
Figure 8. a) Confocal images of MDA-MB-231 cells incubated in phenol-red free complete RMPI medium spiked with DMSO (control, top) and with compound **9** at 100 μM for 4 hours. Images were recorded on Zeiss LSM980-Airyscan confocal microscope using 40x 1.3 NA oil objective. Rhodamine phalloidin was imaged using Alexa-Flour 568 (ex/em 577/603 nm) and compound 9 was imaged using CellTrace calcein violet (ex/em 400/452 nm). Scale bar = 50 μm. b) Comparison of fluorescence intensity and cell area between control and all samples treated with compound **9** after 1, 2 and 4 hours. (ns = not significant, $p > 0.05$, **** = statistically significant, $p < 0.0001$).

ChemBioChem

Research Article
doi.org/10.1002/cbic.202400759

Chemistry Europe
European Chemical
Societies Publishing

NMR, IR, HRMS, EA, CV, and scXRD where possible. The compounds all exhibit reversible Fc′/Fc′$^+$ redox couples ($E_{1/2} = 0.63$–0.66 V) and a reduction at potentials below -1.53 V, which are assigned to the organic part of the β-diketonates. Alkyl substituted β-diketonates are generally more stable towards reduction than their aryl substituted counterparts, with the anthracenyl substituted compound **9** being the least stable.

The compounds cytotoxicity values were determined against human cell lines: pancreatic carcinoma (MIA PaCa-2), ovarian adenocarcinoma (A2780), breast adenocarcinomas (MDA-MB-231 and MCF-7) and normal epithelial retinal (ARPE-19). A general trend was observed, where the increase in number of aromatic rings yields an increase in cytotoxicity, e.g., anthracenyl > naphthyl > phenyl > methyl. High cytotoxicity and selectivity values were observed for the triple negative breast cancer cell line, MDA-MD-231, and further cell studies were used to determine modes of action in this cell line.

Due to the low stability of the compounds (2–6 hours), reactive oxygen species (ROS) and cell morphology studies were conducted after 2 hours of incubation. Whilst the compounds exhibit increased ROS after 2 hours, the morphology of the cells remained unchanged for all compounds, except for the methyl substituted compound **1** which induced cell shrinkage and retraction of lamellipodia, which are signs of cellular stress and possibly early-stage apoptosis.

As compound **9** contains an anthracenyl substituent, its fluorescence capabilities were studied. When coupled to the ferrocenyl, the fluorescence was quenched, however, an increase in fluorescence intensity was observed over time. In line with the NMR findings, we attribute this to the decomposition of the ferrocenyl moiety, which is prompted by the oxidation of the Fe(II) to Fe(III) and loss of free Cp. Confocal microscopy was used to visualize the uptake of this compound into MDA-MB-231 cells, and the samples exhibit a significantly increased fluorescence in the whole cell. When comparing the samples at different incubation times, no change in fluorescence intensity was observed, demonstrating, that cellular uptake is fast. These results give us a unique insight into the possible decomposition of such pro-drugs and allow us to start determining possible active drugs. However, future studies need to focus on the localization of such molecules within cells, to help us understand possibly cellular targets.

Experimental Section

General Information: Chemicals were obtained from commercial suppliers (Fluorochem, Merck KGaA, Fisher Scientific) and used without further purification. Dried THF was obtained from a solvent purification system (MBraun, MB-SPS 800). The acid esters for the synthesis of compounds **3** and **7** were synthesized according to a standard protocol using sulfuric acid as catalyst.[27] Gibco™ high glucose Dulbecco's Modified Eagle Medium (DMEM) and Gibco™ Roswell Park Memorial Institute (RPMI-1640) medium, sodium pyruvate (1 mM), L-glutamine, Fetal bovine serum (FBS), phosphate buffer solution (PBS), pen-strep and Trypsin-EDTA (0.25%) were all purchased from Fisher Scientific or Merck KGaA. All one-use plastic consumables were purchased from Sarstedt.

^{1}H and ^{13}C{^{1}H} NMRs were recorded either on a Bruker Avance III 400 (Ultrashield 400 Plus) or a Bruker Avance III 500 (Ascent 500) and referenced to TMS using the respective residual solvent signal as secondary standard. Multiplicities are abbreviated as s = singlet, d = doublet, t = triplet, q = quartet, br = broad, m = multiplet or respective combinations. NMRs were assignments are referred to the labelled structures in the *Supporting Information*. IR spectra were measured with a Perkin Elmer Spectrum Two with a UATR Two probe. UV/Vis spectra were obtained using a Jasco V-730 spectrometer equipped with a PAC-743R temperature control unit. Samples for elemental analysis were sent to London Metropolitan University and analyzed using a ThermoFlash 2000 by Thermo Scientific.

High Resolution Mass Spectrometry (HRMS): Samples were dissolved in acetonitrile and analyzed in positive ion mode in a mass scan range of 50–3000 *m/z* through direct infusion on a Bruker Compact Q-TOF mass spectrometer. Ionization settings: nebulizer gas 0.3 bar, desolation gas (N_2) 4 L/min, dry temperature 200°C, capillary voltage of -4000 V, capillary end plate offset of 500 V. The calibration was done with sodium formate (10 mM).

Cyclic Voltammetry (CV): A Metrohm Autolab PGSTAT30 potentiostat combined with the Nova software package (Metrohm, Version 2.1.5) was used to conduct CV measurements. A glassy carbon working electrode (diameter = 3 mm) and a glassy carbon rod counter electrode were used. As a reference electrode, a double junction Ag/AgCl electrode was used with a 2 M solution of LiCl in ethanol in the inner compartment and 0.1 M NBu_4PF_6 solution in acetonitrile in the outer compartment. All samples were measured in concentrations of 0.7–0.8 mg/mL in 10 mL of a dried and degassed 0.1 M NBu_4PF_6 solution in acetonitrile. The cyclic voltammograms were corrected using ferrocene as internal standard with the Fc/Fc$^+$ couple at 0.40 V vs SCE (standard calomel electrode).[28] The reversible Fc′/Fc′$^+$ couple was measured between -0.6–1.1 V with scanning speeds of 50, 100, 200, 300 and 500 mV/s. All other voltammograms were obtained using a scanning speed of 100 mV. The potentials were scanned three times and are presented using QtiPlot.

Single crystal X-ray Diffraction (scXRD): A suitable single crystal was selected and immersed in fomblin. The crystal was then mounted to a goniometer head on an XtaLAB Synergy Dualflex, HyPix diffractometer fitted with a Hybrid Pixel Array Detector and a goniometer head, using mirror monochromated Mo–Kα radiation ($\lambda = 0.71073$ Å) source. The crystal was cooled to 100 K by an Oxford cryostream low temperature device.[29] The full data set was recorded and the images processed using CrysAlis Pro.[30] Structure solution by direct methods was achieved through the use SHELXT[31] and SHELXL[32] programs, and the structural model refined by full matrix least squares on F^2 using the program Olex2 v1.5.[33] Hydrogen atoms were placed using idealized geometric positions (with free rotation for methyl groups), allowed to move in a "riding model" along with the atoms to which they were attached, and refined isotropically. Editing of the CIFs and construction of tables of bond lengths and angles were also achieved using Olex2 v1.5. All molecular images were generated using Mercury 4.0.[34]

Deposition Number(s) 2383116 (for **1**), 2375601 (for **3**), 2375603 (for **5**), 2375602 (for **6**), and 2375604 (for **7**) contains the supplementary crystallographic data for this paper. These data are provided free of charge by the joint Cambridge Crystallographic Data Centre and Fachinformationszentrum Karlsruhe Access Structures service.

Synthesis: The acid esters for the synthesis of compounds **3** and **7** were synthesized via a Fisher-Speier esterification reaction using sulfuric acid as a catalyst and isolated by extraction with DCM.[27] 9-Anthracene carbonyl chloride was obtained in quantitative yields

ChemBioChem

Research Article
doi.org/10.1002/cbic.202400759

Chemistry Europe
European Chemical
Societies Publishing

by reacting 9-anthracene carboxylic acid with an excess of oxalyl chloride and catalytic amounts of DMF.[17] Compounds **1**, **2** and **4** have been synthesized following literature procedures.[14–16] Compounds **3** (± 0.44), **5** (± 0.46), **7** (± 0.52), **9** (± 0.95) have elemental analysis hydrogen values which are outside the required $\pm 0.4\%$. Although these results are outside the range viewed as establishing analytical purity, they are provided to illustrate the best values obtained to date. The hydrogen values are lower than expected and this can be explained by the lack of composition aid used in the analysis of the samples, which has been confirmed by the London Metropolitan University EA service. We have provided HRMS for all new samples to prove their successful synthesis and purity.

General procedure for compounds 3–8: Sodium ethoxide (1.4 eq.) was suspended in dried and degassed THF in a Schlenk flask. Acetylferrocene (FcAc, 1.0 eq.) was added, and the mixture stirred for 10 min at room temperature. The respective carboxylic acid ethyl ester (1.02 eq.) was added, and the reaction heated to 70 °C for 3.5–16 h. The reaction progress was monitored by TLC. After completion, the reaction was quenched by adding trifluoroacetic acid (TFA, 1.35 eq.). All following steps were performed under aerobe conditions. Water was added to the reaction solution followed by extractions with DCM (3×25 mL). After drying (brine and sodium sulfate), the solvent was removed *in vacuo*, and the crude products purified by flash chromatography to obtain orange-red powders.

Synthesis of compound 9: A solution of FcAc (284 mg, 1.25 mmol, 1 eq.) in dried and degassed THF (10 mL) was cooled to 0 °C in a Schlenk flask. A solution of sodium bis(trimethylsilyl)amide (2.5 mL 1 M solution, 2.49 mmol, 2 eq.), diluted in 10 mL THF, was then added dropwise over 20 min. The reaction was stirred at 0 °C for additional 10 min. A solution of anthracene-9-carboxylic acid chloride (300 mg, 1.25 mmol, 1 eq.) was added slowly per cannula and the reaction kept for 1 h at 0 °C. The mixture was warmed to room temperature and stirred overnight. The reaction was then quenched by addition of TFA (186 μL, 2.43 mmol, 1.95 eq.) and concentrated to a volume of approximately 10 mL. After addition of water (50 mL), the product was extracted using DCM (3×25 mL), the organic layers combined and dried with sodium sulfate, and the solvent removed *in vacuo*. The crude product was purified by flash chromatography to obtain a bright red powder.

Compound 3: **Scale**: 4.39 mmol FcAc. **Solvent (chromatography)**: 9/1 hexane/ethyl acetate; **Yield**: 620 mg, 1.79 mmol, 41%; **^{1}H NMR (400 MHz, acetone-d$_6$, 298 K, ppm): δ** 15.98, (br. s, 1H, enol OH), 7.39–7.32 (m, 4H, H$_{16,17,19,20}$), 7.29–7.25 (m, 1H, H$_{18}$), 6.00 (s, 1H, H$_2$), 4.81 (t, 2H, $^3J(^1H-^1H)=$1.9 Hz, H$_{5,8}$), 4.55 (t, 2H, $^3J(^1H-^1H)=$1.9 Hz, H$_{6,7}$), 4.16 (s, 5H, H$_{9-13}$), 3.64 (s, 2H, H$_{14}$); *Identifiable signals of the keto form:* δ 7.39–7.32 (m, 4H, H$_{16,17,19,20}$), 7.29–7.25 (m, 1H, H$_{18}$), 4.76 (t, 2H, $^3J(^1H-^1H)=$1.9 Hz, H$_{5,8}$), 4.58 (t, 2H, $^3J(^1H-^1H)=$1.9 Hz, H$_{6,7}$), 4.25 (s, 5H, H$_{9-13}$), 4.00 (s, 2H, H$_{2 or 14}$), 3.95 (s, 2H, H$_{2 or 14}$); **^{13}C{^{1}H} NMR (100 MHz, acetone-d$_6$, 298 K, ppm): δ** 130.1 (CH, C$_{16,20 or 17,19}$), 129.4 (CH, C$_{16,20 or 17,19}$), 127.6 (CH, C$_{18}$), 97.8 (CH, C$_2$), 73.0 (CH, C$_{6,7}$), 71.1 (CH, C$_{9-13}$), 69.5 (CH, C$_{5,8}$), 44.6 (CH$_2$, C$_{14}$); *Identifiable signals of the keto form:* δ 70.7 (CH, C$_{9-13}$). Ratio enol/keto (1/0.28); **IR (ATR, cm^{-1})**: $\tilde{v}=$3118 (w, CH–Cp), 2937 (w, CH–CH$_2$), 1574 (vs, br, CO-acac), 499 (vs), 483 (vs), 464 (m, Cp–Fe–Cp); **HRMS (ESI)** *m/z* calculated for C$_{20}$H$_{18}$FeO$_2$: [M]$^+$ 346.0651, [M+Na]$^+$ 369.0549, **Found**: [M]$^+$ 346.0649, [M+Na]$^+$ 369.0541; **EA Analysis calculated for C$_{20}$H$_{18}$FeO$_2$**: C 69.39, H 5.24%, **Found**: C 69.37, H 4.80%.

Compound 5: **Scale**: 3.29 mmol FcAc. **Solvent (chromatography)**: 10/1 hexane/ethyl acetate; **Yield**: 352 mg, 0.888 mmol, 27.0%; **^{1}H NMR (500 MHz, acetone-d$_6$, 1 vol% TMS, 298 K, ppm): δ** 16.09 (s br, 1H, enol OH), 8.17 (ddd, 1H, $^3J(^1H-^1H)=$8.5 Hz, $^4J(^1H-^1H)=$1.7, 0.8 Hz, H$_{22}$), 7.95 (ddd, 1H, $^3J(^1H-^1H)=$8.0 Hz, $^4J(^1H-^1H)=$1.5, 0.7 Hz,

H$_{17 or 20}$), 7.89 (app. dt, 1H, $^3J(^1H-^1H)=$8.1 Hz, $^4J(^1H-^1H)=$1.2 Hz, H$_{17 or 20}$), 7.59 – 7.50 (m, 4H, H$_{18,19,23,24}$), 5.90 (s, 1H, H$_2$), 4.69 (t, 2H, $^3J(^1H-^1H)=$2.0 Hz, H$_{5,8}$), 4.50 (t, 2H, $^3J(^1H-^1H)=$2.0 Hz, H$_{6,7}$), 4.15 (s, 2H, H$_{14}$), 4.03 (s, 5H, H$_{9-13}$); *Identifiable signals of the keto form:* δ 8.05–8.07 (m, 1H, H$_{22}$), 7.92 – 7.90 (m, 1H, H$_{17 or 20}$), 7.85 – 7.87 (m, 1H, H$_{17 or 20}$), 7.45 – 7.59 (m, 4H, H$_{18,19,23,24}$), 4.78 (t, 2H, $^3J(^1H-^1H)=$2.0 Hz, H$_{5,8}$) 4.58 (t, 2H, $^3J(^1H-^1H)=$2.0 Hz, H$_{6,7}$), 4.46 (s, 2H, H$_{14}$), 4.15 (s, 5H, H$_{9-13}$), 4.07 (s, 2H, H$_2$); **^{13}C{^{1}H} NMR (100 MHz, acetone-d$_6$, 298 K, ppm): δ** 193.1 (Q CO, C$_{1 or 3}$), 189.0 (Q CO, C$_{1 or 3}$), 134.9 (CH, C$_{15,16 or 21}$), 133.4 (CH, C$_{15,16 or 21}$), 133.2 (CH, C$_{15,16 or 21}$), 129.5 (C$_{17 or 20}$), 129.0 (CH, C$_{18,19,23,24}$), 127.0 (CH, C$_{18,19,23,24}$), 126.6 (CH, C$_{18,19,23,24}$), 126.5 (CH, C$_{18,19,23,24}$), 128.6 (CH, C$_{17 or 20}$), 125.1 (C$_{22}$), 97.9 (CH, C$_2$), 78.3 (Q, C$_4$), 72.9 (CH, C$_{6,7}$), 71.0 (CH, C$_{9-13}$) 69.3 (CH, C$_{5,8}$), 42.2 (CH, C$_{14}$); *Identifiable signals of the keto form:* δ 202.9 (Q CO, C$_{1 or 3}$), 198.4 (Q CO, C$_{1 or 3}$), 134.8 (CH, C$_{15,16 or 21}$), 133.5 (CH, C$_{15,16 or 21}$), 132.4 (CH, C$_{15,16 or 21}$) 129.4 (CH, C$_{17-20,23 or 24}$), 129.4 (CH, C$_{17-20,23 or 24}$), 128.6 (CH, C$_{17-20,23 or 24}$), 127.0 (CH, C$_{17-20,23 or 24}$), 126.6 (CH, C$_{17-20,23 or 24}$), 126.4 (CH, C$_{17-20,23 or 24}$), 125.4 (CH, C$_{22}$), 80.2 (Q, C$_4$), 73.5 (CH, C$_{6,7}$), 70.7 (CH, C$_{9-13}$) 70.4 (CH, C$_{5,8}$), 53.8 (CH$_2$, C$_{14}$), 49.0 (CH$_2$, C$_2$); Ratio enol/keto (1/0.24); **IR (ATR, cm^{-1}): $\tilde{v}=$**3108 (w, CH–Cp), 2926 (w, CH–CH$_2$), 1555 (vs, br, CO-acac), 497 (vs), 483 (vs), 465 (m, sh, Cp–Fe–Cp); **HRMS (ESI)** *m/z* calculated for C$_{24}$H$_{20}$FeO$_2$: [M]$^+$ 396.0807, [M+Na]$^+$ 419.0705, **Found**: [M]$^+$ 396.0810, [M+Na]$^+$ 419.0707; **EA Analysis calculated for C$_{24}$H$_{20}$FeO$_2$**: C 72.74, H 5.09%, **Found**: C 72.81, H 4.63%.

Compound 6: **Scale**: 3.29 mmol FcAc. **Solvent (chromatography)**: 12/1 hexane/ethyl acetate; **Yield**: 618 mg, 1.62 mmol, 49%; **^{1}H NMR (400 MHz, acetone-d$_6$, 298 K, ppm): δ** 8.68 (d, 1H, $^4J(^1H-^1H)=$ 2.0 Hz, H$_{15}$), 8.13 (dd, 1H, $^3J(^1H-^1H)=$8.7 Hz, $^4J(^1H-^1H)=$2.0 Hz, H$_{23}$), 8.10–8.06 (m, 1H, H$_{17 or 20}$) 8.03 (d, 1H, $^3J(^1H-^1H)=$8.7 Hz, H$_{22}$), 8.01–7.97 (m, 1H, H$_{17 or 20}$), 7.62 (app. tt, 2H, $^3J(^1H-^1H)=$6.9, 5.2 Hz, H$_{18,19}$), 6.93 (s, 1H, H$_2$), 5.08 (t, 2H, $^3J(^1H-^1H)=$1.9 Hz, H$_{5,8}$), 4.64 (t, 2H, $^3J(^1H-^1H)=$1.9 Hz, H$_{6,7}$), 4.25 (s, 5H, H$_{9-13}$); *Identifiable signals of the keto form:* δ 8.76 (d, 1H, $^4J(^1H-^1H)=$1.7 Hz, H$_{15}$), 4.89 (t, 2H, $^3J(^1H-^1H)=$1.9 Hz, H$_{5,8}$), 4.65 (s, 2H, H$_2$), 4.61 (t, 2H, $^3J(^1H-^1H)=$1.9 Hz, H$_{6,7}$), 4.28 (s, 5H, H$_{9-13}$); **^{13}C{^{1}H} NMR (100 MHz, acetone-d$_6$, 295 K, ppm): δ** 195.5 (Q, C$_{1 or 3}$), 179.9 (Q, C$_{1 or 3}$), 136.0 (CH, C$_{16 or 21}$), 133.9 (CH, C$_{16 or 21}$), 133.3 (Q, C$_{14}$), 130.1 (CH, C$_{15,17-20,22 or 23}$), 129.2 (CH, C$_{15,17-20,22 or 23}$), 128.8 (CH, C$_{15,17-20,22 or 23}$), 128.6 (CH, C$_{15,17-20,22 or 23}$), 128.4 (CH, C$_{15,17-20,22 or 23}$), 127.7 (CH, C$_{15,17-20,22 or 23}$), 124.2 (CH, C$_{15,17-20,22 or 23}$), 95.1 (CH, C$_2$), 79.3 (Q, C$_4$) 73.3 (CH, C$_{6,7}$), 71.7 (CH, C$_{9-13}$), 69.8 (CH, C$_{5,8}$). *Identifiable signals of the keto form:* δ 73.4 (CH, C$_{6,7}$), 70.7 (CH, C$_{9-13}$), 70.6 (CH, C$_{5,8}$); Ratio enol/keto (1/0.08); **IR (ATR, cm^{-1})**: $\tilde{v}=$3111 (w, CH–Cp), 1600 (m), 1539 (vs, br, CO-acac), 502 (vs), 487 (s), 468 (vs, Cp–Fe–Cp); **HRMS (ESI)** *m/z* calculated for C$_{23}$H$_{18}$FeO$_2$: [M]$^+$ 382.0651, [M+Na]$^+$ 405.0549, **Found**: [M]$^+$ 382.0651, [M+Na]$^+$ 405.0549; **Analysis calculated for C$_{23}$H$_{18}$FeO$_2$**: C 72.27, H 4.75%, **Found**: C 72.29, H 4.44%.

Compound 7: **Scale**: 4.39 mmol FcAc. **Solvent (chromatography)**: 11/1 hexane/ethyl acetate; **Yield**: 300 mg, 0.71 mmol, 16%; **^{1}H NMR (400 MHz, acetone-d6, 298 K, ppm): δ** 16.16 (s br, 1H, enol OH), 7.40–7.34 (m, 8H, H$_{16,17,19,20}$), 7.31–7.26 (m, 2H, H$_{18}$), 6.02 (s, 1H, H$_2$), 5.15 (s, 1H, H$_{14}$), 4.78 (t, 2H, $^3J(^1H-^1H)=$1.9 Hz, H$_{5,8}$), 4.55 (t, 2H, $^3J(^1H-^1H)=$1.9 Hz, H$_{6,7}$), 4.14 (s, 5H, H$_{9-13}$); *Identifiable signals of the keto form:* δ 7.40–7.34 (m, 8H, H$_{16,17,19,20}$), 7.31–7.26 (m, 2H, H$_{18}$), 5.60 (s, 1H, H$_{14}$), 4.74 (t, 2H, $^3J(^1H-^1H)=$1.9 Hz, H$_{5,8}$), 4.57–4.56 (m, 2H, H$_{6,7}$), 4.21 (s, 5H, H$_{9-13}$), 4.04 (s, 2H, H$_2$); **^{13}C{^{1}H} NMR (100 MHz, acetone-d$_6$, 298 K, ppm): δ** 192.8 (Q, C$_{1 or 3}$), 190.7 (Q, C$_{1 or 3}$), 141.1 (Q, C$_{15}$), 129.9 (CH, C$_{16,20 or 17,19}$), 129.3 (CH, C$_{16,20 or 17,19}$), 127.8 (CH, C$_{18}$), 99.0 (CH, C$_2$), 78.2 (Q, C$_4$), 73.1 (CH, C$_{6,7}$), 71.1 (CH, C$_{9-13}$), 69.4 (CH, C$_{5,8}$), 59.9 (CH, C$_{14}$); *Identifiable signals of the keto form:* δ 203.4(Q, C$_{1 or 3}$), 198.1 (Q, C$_{1 or 3}$), 139.4 (Q, C$_{15}$), 130.2 (CH, C$_{16,17,19 or 20}$), 129.4 (CH, C$_{16,17,19 or 20}$), 127.8 (CH, C$_{18}$), 73.5 (CH, C$_{6,7}$), 70.7 (CH, C$_{9-13}$), 70.4 (CH, C$_{5,8}$), 65.0 (CH, C$_{14}$), 54.1 (CH$_2$, C$_2$); Ratio enol/keto (1/0.24); **IR (ATR, cm^{-1})**: $\tilde{v}=$3112 (w, CH–Cp), 2888 (w, CH-aliphatic), 1596 (vs,

ChemBioChem

Research Article
doi.org/10.1002/cbic.202400759

Chemistry Europe
European Chemical
Societies Publishing

br, CO-acac), 498 (vs), 482 (vs), 463 (s, Cp–Fe–Cp); **HRMS (ESI) _m/z_ calculated for $C_{26}H_{22}FeO_2$:** $[M]^+$ 422.0960, $[M+Na]^+$ 445.0862, **Found**: $[M]^+$ 422.0960, $[M+Na]^+$ 445.0855; **EA Analysis calculated for $C_{26}H_{22}FeO_2$:** C 73.95, H 5.25 %, **Found**: C 73.64, H 4.73 %.

Compound 8: Scale: 3.29 mmol FcAc. **Solvent (chromatography):** 12/1 hexane/ethyl acetate; **Yield:** 320 mg, mmol, 24 %; **^{1}H NMR (500 MHz, acetone-d_6, 1 vol% TMS, 300 K, ppm): δ** 8.29 (app. dt, 1H, $^4J(^1H–^1H) = 1.8$ Hz, $^5J(^1H–^1H) = 0.4$ Hz, H_{18}), 8.06 (ddd, 1H, ^3J-$(^1H–^1H) = 7.8$ Hz, $^4J(^1H–^1H) = 1.8$, 1.1 Hz, $H_{17 \text{ or } 19}$), 7.86 (ddd, 1H, $^3J(^1H–^1H) = 7.8$ Hz, $^4J(^1H–^1H) = 1.8$, 1.1 Hz, $H_{17 \text{ or } 19}$), 7.75–7.73 (m, 2H, $H_{21,25}$), 7.62 (app. dt, 1H, $^3J(^1H–^1H) = 7.8$ Hz, $^5J(1H\text{-}1H) = 0.4$ Hz, H_{15}), 7.53–7.50 (m, 2H, $H_{22,24}$, 7.44–7.40 (m, 1H, H_{23}), 6.88 (s, 1H, H_2), 5.07 (t, 2H, $^3J(^1H–^1H) = 1.9$ Hz, $H_{5,8}$), 4.63 (t, 2H, $^3J(^1H–^1H) = 1.9$ Hz, $H_{6,7}$), 4.24 (s, 5H, $H_{9–13}$); _Identifiable signals of the keto form:_ δ 8.36 (app. dt, $^4J(^1H–^1H) = 1.9$ Hz, $^5J(^1H–^1H) = 0.5$ Hz, H_{18}), 7.94 (ddd, 1H, $^3J(^1H–^1H) = 7.7$ Hz, $^4J(^1H–^1H) = 1.9$, 1.1 Hz, $H_{17 \text{ or } 19}$), 4.88 (t, 2H, $^3J(^1H–^1H) = 1.8$ Hz, $H_{5,8}$), 4.61 (t, 2H, $^3J(^1H–^1H) = 1.8$ Hz, $H_{6,7}$), 4.60 (s, 2H, H_2), 4.26 (s, 5H, H9–13); **$^{13}C\{^1H\}$ NMR (100 MHz, acetone-d_6, 298 K, ppm): δ** 195.7 (Q, $C_{1 \text{ or } 3}$), 180.1 (Q, $C_{1 \text{ or } 3}$), 142.7 (Q, $C_{14,16 \text{ or } 20}$), 141.2 (Q, $C_{14,16 \text{ or } 20}$), 136.7 (Q, $C_{14,16 \text{ or } 20}$), 131.3 (CH, $C_{17 \text{ or } 19}$), 130.2 (C_{15}), 129.9 ($C_{22,24}$), 128.6 (C_{23}), 128.0 ($C_{21,25}$), 126.6 ($C_{17 \text{ or } 19}$), 126.0 (C_{18}), 94.9 (CH, C_2), 79.2 (Q, C_4), 73.3 (CH, $C_{6,7}$), 71.1 (CH, $C_{9–13}$), 69.8 (CH, $C_{5,8}$); _Identifiable signals of the keto form:_ δ 73.4 (CH, $C_{6,7}$), 70.7 (CH, $C_{9–13}$), 69.8 (CH, $C_{5,8}$); **Ratio enol/keto (1/0.06); IR (ATR, cm^{-1}):** $\tilde{v} = 3107$ (w, CH–Cp), 1592 (s, br, CO-acac), 500 (vs), 484 (s), 470 (m, Cp–Fe–Cp); **HRMS(ESI) m/z calculated for $C_{25}H_{20}FeO_2$:** $[M]^+$ 408.0807, $[M+Na]^+$ 431.0705, **Found:** $[M]^+$ 408.0805, $[M+Na]^+$ 431.0702; **EA Analysis calculated for $C_{25}H_{20}FeO_2$:** C 73.55, H 4.94 %, **Found:** C 73.35, H 4.82 %.

Compound 9: Scale: 1.25 mmol FcAc. **Solvent (chromatography):** 10/1 to 7/1 hexane/ethyl acetate; **Yield:** 320 mg, 0.740 mmol, 59 %; **^{1}H NMR (400 MHz, acetone-d_6, 298 K, ppm): δ** 8.73 (s, 1H, H_{21}), 8.28–8.25 (m, 2H, $H_{16,26}$), 8.18–8.15 (m, 2H, $H_{19,23}$), 7.63–7.55 (m, 4H, $H_{17,18,24,25}$), 6.37 (s, 1H, H_2), 5.03 (t, 2H, $^3J(^1H–^1H) = 2.0$ Hz, $H_{5,8}$), 4.65 (t, 2H, $^3J(^1H–^1H) = 2.0$ Hz, $H_{6,7}$), 4.33 (s, 5H, $H_{9–13}$); **$^{13}C\{^1H\}$ NMR (100 MHz, acetone-d_6, 298 K, ppm): δ** 132.2 (Q, $C_{20,22}$), 129.5 (CH, C_{21}), 129.5 (CH, $C_{19,23}$), 129.4 (Q, $C_{15,27}$), 127.6, 126.5 (CH, $C_{17,18,24,25}$), 126.3 (CH, $C_{16,26}$), 103.4 (CH, C_2), 77.6 (Q, C_4), 73.7 (CH, $C_{6,7}$), 71.2 (CH, $C_{9–13}$), 70.0 (CH, $C_{5,8}$); **No keto form detected. IR (ATR, cm^{-1}):** $\tilde{v} = 3112$ (w, sh, CH–Cp), 1592 (vs, br, CO-acac), 496 (vs), 484 (vs), 470 (m, sh, Cp–Fe–Cp); **HRMS (ESI) _m/z_ calculated for $C_{27}H_{20}FeO_2$:** $[M]^+$ 432.0808, $[M+Na]^+$ 455.0705, **Found:** $[M]^+$ 432.0802, $[M+Na]^+$ 455.0701; **EA Analysis calculated for $C_{27}H_{20}FeO_2$:** C 75.02, H 4.66 %, **Found:** C 75.26, H 3.71 %.

Stability Studies: NMR samples of compounds **1–9** (5 mg/mL) were prepared in either 100 % $(CD_3)_2SO$ or 90 % $(CD_3)_2SO$ and 10 % D_2O, and spectra recorded using Bruker Avance III 400 (Ultrashield 400 Plus) at initial (ca. 5 mins), 10, 20 and 60 mins, 2, 6, 12, 24, 48, 72 and 96 h time points.

Cell viability assay: All cytotoxicity assays were conducted using human cell lines: pancreatic carcinoma (MIA PaCa-2), ovarian adenocarcinoma (A2780), breast adenocarcinomas (MDA-MB-231 and MCF-7) and normal epithelial retinal (ARPE-19) cell lines and were routinely maintained as monolayer cultures in appropriate complete medium. MIA PaCa-2, MCF-7 ARPE-19 were cultured in high glucose DMEM complete medium with 10 % FBS, 1 mM sodium pyruvate, 2 mM and 1 % pen-strep, whilst and A2780 and MDA-MB-231 were cultured in RPMI-1640 complete medium (with the same supplements) and grown in either T-25 or T-75 flasks at 37 °C and 5 % CO_2. Prior to chemosensitivity studies, cell monolayers were passaged using Trypsin-EDTA (0.05–0.25 %) and diluted to a concentration of 0.5–1×10^4 cells/mL for 96 h assays, or 4×10^4 cells/mL for 24 h assays. All assays were conducted using 96-well plates, in which 100 μL of the cell suspension were added for 24 h at 37 °C

and 5 % CO_2, and then 100 μL of compound/media dilutions for 96 h (24 h against MDA-MB-231 only). All compound stocks were made using sterile DMSO at 50 mM prior to dilution. After 96 h, MTT (3-(4,5-dimethylthiazol-2-yl)-2,5-diphenyltetrazolium bromide (20 μL, 5 mg/mL in PBS) was added to each well and incubated for a further 3 h at 37 °C and 5 % CO_2. All solutions were then removed via pipette and DMSO (150 μL) added to each well and the absorbance measured at 540 nm using a ClarioStar spectrophotometer microplate reader. Results were plotted on a logarithmic scale, and the half maximal inhibitory concentration (IC_{50}) determined from triplicate of triplicate repeats (n = 9) and reported as an $IC_{50} \pm$ Standard Deviation (SD).

Reactive Oxygen Species: MDA-MB-231 cells (maintained as described above) were seeded in a 96-well optical bottom plates at 40,000 cells/mL in phenol-red free complete RPMI medium (100 μL) and incubated at 37 °C and 5 % CO_2 for 2 days, after which phenol-red free complete RPMI medium (100 μL) spiked with the compounds or cisplatin (100 μM) were added. The cells were incubated for 2 h and after this time the medium removed and the wells washed with PBS (100 μL). H_2DCFDA (20 μL) in PBS:DMSO (91:3) was added to give a final dye concentration of 20 μM. The cells were incubated with the dye for 30 min, after which the medium was removed, and the wells gently washed with PBS (2×200 μL) and phenol-red free complete RMPI medium (100 μL) was added. The cells were imaged using an Observer-7 microscope, excitation 494 nm and emission 512 nm.

Cell Morphology: MDA-MB-231 cells (maintained as described above) were seeded a 12-well plate on a glass slide at 40,000 cells/mL. Cell suspensions were maintained in phenol-red free complete RPMI medium and incubated at 37 °C and 5 % CO_2 for 24 h, after which phenol-red free complete RPMI (500 μL) spiked with DMSO (0.4 %, control), compounds or cisplatin (100 μM) was added. The cells were incubated for 2 or 8 h followed by washing once with PBS (500 μL) and addition of Image-iT® solution (500 μL, Thermofisher Scientific) containing 3 % PFA and 0.35 % glutaraldehyde. The slides were kept at room temperature for 1 h and then stored at 4 °C overnight. After removing the fixing solution, the slides are washed with PBS (5×500 μL) and fixed with 1 % aqueous OsO_4 at 4 °C (300 μL). The slides are further washed 0.1 M sodium cacodylate buffer (5×300 μL) and dried using sequential ethanol solutions (25, 50, 75 and 100 %, 1×300 μL). The cover slips were mounted on adhesive carbon fitted on aluminium stubs and then gold coated using a SC7640 Gold sputter coater manufactured by Quorum Technologies. Samples were measured on a GeminiSEM 300 field emission scanning electron microscope (Zeiss GmbH) using 2 keV acceleration and the signal was recorded by the secondary electron detector.

Fluorescence: Samples of compound **9** at a concentration of 20 μM were prepared either in neat DMSO or by adding the compound dissolved in DMSO to complete RPMI medium (final concentration of DMSO 5 %). The samples were left open to allow oxygen to enter and measured after multiple points in time on a Spectrofluorometer FS5 (Edinburgh Instruments).

Confocal Microscopy: MDA-MB-231 cells (maintained as described above) were seeded in a 12-well plate on glass slides at 40,00 cells/mL. Cell suspensions were maintained in phenol-red free complete RPMI medium and incubated at 37 °C and 5 % CO_2 for 24 h, after which complete RPMI medium (500 μL) spiked with compound **9** (100 μM) was added. The cells were incubated for 1, 2 and 4 h followed by washing with PBS (500 μL). The samples were fixed with PFA (4 % in PBS, 500 μL) for 10 mins at room temperature and permeabilized with 0.1 % TritonX (1000 μL) for 10 mins before being incubated in rhodamine phalloidin (1:200) (Thermofisher Scientific) in 3 % BSA (750 μL) for 45 min at room temperature. Cells were

mounted onto slides using Vectashield mounting medium (Vector Laboratories Ltd.) and imaged on Zeiss LSM980-Airyscan confocal microscope using 40x 1.3 NA oil objective or 100x 1.4 NA oil objective. Rhodamine phalloidin was imaged using Alexa-Flour 568 (dye name: AF568) (excitation 577 nm and emission 603 nm) and compound **9** was imaged using CellTrace calcein violet (dye name: CeTCV) (excitation 400 nm and emission 452 nm). Images were analyzed in Fiji ImageJ 1.53 t. A region of interest was drawn around the cell edge, using the rhodamine phalloidin image. These regions of interest were saved and used to measure the cell area and fluorescence intensity of the green image, using the measure tool.

Data Analysis: Statistical analysis of the cytotoxicity results was conducted using Student's t-test; $p > 0.05$ being considered not significant and $p < 0.05$ being significant. For confocal image analysis, the results are presented as mean $\pm$ SEM. One-way ANOVA was performed, followed by a Tukey's multiple comparison post-hoc test; $p > 0.05$ being considered not significant and $p < 0.0001$ being significant. All statistical analysis was performed using GraphPad Prism 9.

Conflict of Interests

The authors declare no conflict of interest.

Data Availability Statement

The data that support the findings of this study are available in the supplementary material of this article.

[1] N. Abbaspour, R. Hurrell, R. Kelishadi, *J. Res. Med. Sci.* **2014**, *19*, 164–174.
[2] T. G. DeLoughery, *Acta Haematol.* **2019**, *142*, 8–12.
[3] G. Papanikolaou, K. Pantopoulos, *Toxicol. Appl. Pharmacol.* **2005**, *202*, 199–211.
[4] a) U. Rauf, G. Shabir, S. Bukhari, F. Albericio, A. Saeed, *Molecules* **2023**, *28*, 5765; b) L. V. Snegur, *Inorganics* **2022**, *10*, 226.
[5] B. S. Ludwig, J. D. G. Correia, F. E. Kühn, *Coord. Chem. Rev.* **2019**, *396*, 22–48.
[6] S. Peter, B. A. Aderibigbe, *Molecules* **2019**, *24*, 3604.
[7] L. Cosimbescu, X. Wei, M. Vijayakumar, W. Xu, M. L. Helm, S. D. Burton, C. M. Sorensen, J. Liu, V. Sprenkle, W. Wang, *Sci. Rep.* **2015**, *5*, 14117.
[8] P. Köpf-Maier, H. Köpf, E. W. Neuse, *J. Cancer Res. Clin. Oncol.* **1984**, *108*, 336–340.
[9] G. Jaouen, A. Vessières, S. Top, *Chem. Soc. Rev.* **2015**, *44*, 8802–8817.
[10] S. Top, J. Tang, A. Vessières, D. Carrez, C. Provot, G. Jaouen, *Chem. Commun.* **1996**, *8*, 955–956.
[11] T. Schilling, K. B. Keppler, M. E. Heim, G. Niebch, H. Dietzfelbinger, J. Rastetter, A. R. Hanauske, *Invest. New Drugs* **1996**, *13*, 327–332.
[12] V. Boscaro, A. Barge, A. Deagostino, E. Ghibaudi, E. Laurenti, D. Marabello, E. Diana, M. Gallicchio, *Molecules* **2021**, *26*, 5534.
[13] R. Wilken, M. S. Veena, M. B. Wang, E. S. Srivatsan, *Mol. Cancer* **2011**, *10*, 12.
[14] M. Allison, D. Wilson, C. M. Pask, P. C. McGowan, R. M. Lord, *ChemBioChem* **2020**, *21*, 1988–1996.
[15] M. Allison, P. Caramés-Méndez, B. J. Hofmann, C. M. Pask, R. M. Phillips, R. M. Lord, P. C. McGowan, *Organometallics* **2023**, *42*, 1869–1881.
[16] M. Allison, P. Caramés-Méndez, C. M. Pask, R. M. Phillips, R. M. Lord, P. C. McGowan, *Chem. Eur. J.* **2021**, *27*, 3737–3744.
[17] G. W. H. Wurpel, A. M. Brouwer, I. H. M. van Stokkum, A. Farran, D. A. Leigh, *J. Am. Chem. Soc.* **2001**, *123*, 11327–11328.
[18] C. De Luca, D. Zanetti, T. Battisti, R. R. Ferreira, S. Lopez, A. H. McMillan, S. C. Lesher-Pérez, L. Maggini, D. Bonifazi, *Chem. Eur. J.* **2023**, *29*, e202302129.
[19] Deposition Numbers 2375601–2375604 and 2383116 contains the supplementary crystallographic data for this paper. These data are provided free of charge by the joint Cambridge Crystallographic Data Centre and Fachinformationszentrum Karlsruhe Access Structures service.
[20] A. Gomes, E. Fernandes, J. L. F. C. Lima, *J. Biochem. Biophys. Methods* **2005**, *65*, 45–80.
[21] H. Nakamura, K. Takada, *Cancer Sci.* **2021**, *112*, 3945–3952.
[22] M. Franchi, Z. Piperigkou, K.-A. Karamanos, L. Franchi, V. Masola, *Cells* **2020**, *9*, 2031.
[23] S. Fery-Forgues, B. Delavaux-Nicot, *J. Photochem. Photobiol. A* **2000**, *132*, 137–159.
[24] A. G. Mirochnik, A. Yu, Beloliptsev, E. V. Fedorenko, *ChemistrySelect* **2020**, *5*, 710–716.
[25] D. Musib, M. Pal, M. K. Raza, M. Roy, *Dalton Trans.* **2020**, *49*, 10786–10798.
[26] S. Banerjee, I. Pant, I. Khan, P. Prasad, A. Hussain, P. Kondaiah, A. R. Chakravarty, *Dalton Trans.* **2015**, *44*, 4108–4122.
[27] P. Wang, A. V. Bay, E. J. Farnam, K. A. Scheidt, *Adv. Synth. Catal.* **2023**, *365*, 2361–2366.
[28] N. G. Connelly, W. E. Geiger, *Chem. Rev.* **1996**, *96*, 877–910.
[29] J. Cosier, A. M. Glazer, *J. Appl. Crystallogr.* **1986**, *19*, 105–107.
[30] O. D. CrysAlis Pro, 171.43.124a, Agilent Technologies UK Ltd, Yarnton, England, **2019**.
[31] G. M. Sheldrick, *Acta Crystallogr.* **2015**, *A71*, 3–8.
[32] G. M. Sheldrick, *Acta Crystallogr. Sect. C* **2015**, *71*, 3–8.
[33] O. V. Dolomanov, L. J. Bourhis, R. J. Gildea, J. A. K. Howard, H. Puschmann, *J. Appl. Crystallogr.* **2009**, *42*, 339–341.
[34] C. F. Macrae, I. Sovago, S. J. Cottrell, P. T. A. Galek, P. McCabe, E. Pidcock, M. Platings, G. P. Shields, J. S. Stevens, M. Towler, P. A. Wood, *J. Appl. Crystallogr.* **2020**, *53*, 226–235.